

# A correlative spatiotemporal microscale study of calcium phosphate formation and transformation within an alginate hydrogel matrix

Sindre H. Bjørnøy<sup>a</sup>, David C. Bassett<sup>a</sup>, Seniz Ucar<sup>b</sup>, Berit L. Strand<sup>c</sup>,  
Jens-Petter Andreassen<sup>b</sup>, Pawel Sikorski<sup>a,\*</sup>

<sup>a</sup>*Department of Physics, NTNU, Norwegian University of Science and Technology, 7491 Trondheim, Norway*

<sup>b</sup>*Department of Chemical Engineering, NTNU, Norwegian University of Science and Technology, 7491 Trondheim, Norway*

<sup>c</sup>*Department of Biotechnology, NTNU, Norwegian University of Science and Technology, 7491 Trondheim, Norway*

---

## Abstract

The modification of soft hydrogels with hard inorganic components is a method used to form composite materials with application in non-load-bearing bone tissue engineering. The inclusion of an inorganic component may provide mechanical enhancement, introduce osteoconductive or osteoinductive properties, or change other aspects of interactions between native or implanted cells and the material. A thorough understanding of the interactions between such components is needed to improve the rational design of biomaterials. Here, we report a detailed investigation of the formation and transformation process of calcium phosphate mineral within an alginate hydrogel matrix. A combination of optical microscopy, confocal Raman microspectroscopy and electron microscopy was used to investigate the spatial distribution, morphology and crystal phase of the calcium phosphate mineral, as well as to study transformation of the mineral phases during the hydrogel mineralization process and upon incubation in a simulated body fluid. It was found, that under the conditions used in this

---

\*Corresponding author

*Email addresses:* `sindre.bjornoy@ntnu.no` (Sindre H. Bjørnøy),  
`david.bassett@ntnu.no` (David C. Bassett), `seniz.ucar@ntnu.no` (Seniz Ucar),  
`berit.l.strand@ntnu.no` (Berit L. Strand), `jens-petter.andreassen@ntnu.no` (Jens-Petter Andreassen), `pawel.sikorski@ntnu.no` (Pawel Sikorski)

work, mineral initially formed as a metastable amorphous calcium phosphate phase (ACP). The ACP particles had a distinctive spherical morphology and transformed within minutes into brushite in the presence of brushite seed crystals or into octacalcium phosphate, when no seeds were present in the hydrogel matrix. Incubation of brushite-alginate composites in simulated body fluid resulted in formation of hydroxyapatite. The characterization strategy presented here allows for non-destructive, *in situ* observation of mineralization processes in optically transparent hydrogels with little to no sample preparation.

*Keywords:* alginate, hydrogel, raman spectroscopy, calcium phosphate

---

## 1. Introduction

Hydrogels combined with inorganic materials are attractive candidates in the search for an injectable composite material for hard tissue regeneration. The hydrogel can be used as a carrier material for cells, drugs or other bioactive molecules and also act as a scaffold for tissue formation.[1] The inorganic phase provides nucleation sites and the necessary ions for *in vivo* bone formation and also modifies the mechanical properties of the resulting composite material.[2, 3] In cases where calcium phosphate (CaP) has been used as the inorganic phase, hydroxyapatite (HAp) has long been the material of choice due to its similarity to the mineral found in bone.[4–6] However, HAp is thermodynamically stable under *in vivo* conditions, and therefore will not readily dissolve and provide ions for bone formation. Therefore, in recent years, less stable CaP phases such as OCP and brushite (the abbreviation DCPD has been used in sample names and figure legends to indicate brushite) have attracted increasing interest in this regard.[7] These acidic phases are often present in the early stages of precipitation *in vitro*, even at mildly alkaline conditions, as they tend to nucleate more easily than HAp.[8] In the more complex *in vivo* environment, evidence of such precursors has been elusive. Whether this stems from the influence of templating molecules or is due to dehydration or other artifacts during sample preparation is not entirely clear. Peptide motifs from dentin matrix proteins

have been shown to accelerate the formation of crystalline HAp *in vitro*, which supports the first scenario.[9] On the other hand, using *in situ* characterization techniques or minimal sample preparation there have been reports of several non-apatitic precursor phases during early mineralization, including amorphous phosphate (ACP) and OCP.[10] More recently, ACP has been shown to act as a precursor to HAp during osteogenesis within a ceramic tissue engineering scaffold loaded with bone marrow mesenchymal stem cells and implanted in a murine model.[11] Also, cellularly derived ACP nanospheres have been shown to transform into crystalline platelets of HA upon contact with the collagen matrix of continuously mineralizing fin bones of zebrafish.[12] Similar mineralization pathways have also been suggested for other types of biominerals, such as calcium carbonate found in sea urchins and mollusks.[13]

Our group focuses on the formation of alginate-CaP composite materials by counter-diffusion in which mineral is precipitated simultaneously with hydrogel crosslinking. This approach allows control over the resulting CaP phase and has recently been investigated in particular for the formation of HAp and brushite.[14, 15] In order to produce phase pure alginate-brushite composites, seed crystals were used to initiate nucleation, since conditions which normally produce brushite when precipitated in solution, resulted in HAp inside the gel network, irrespective of the precursor concentrations and initial pH.[15] Further investigation into this phenomena revealed an inhibitory effect of alginate on the growth and nucleation of brushite in the presence of small amounts of alginate.[16]

A thorough understanding of CaP formation and transformation processes is essential for both fundamental studies of biomineralization and for the development of synthetic hard tissue engineering scaffold biomaterials. CaP mineralization, although dependent on reaction conditions such as pH and ionic strength, is often dictated by kinetics rather than thermodynamics. In addition, the crystallization process may be influenced by both (bio)organic molecules and spatial confinement.[17–25] This represents a particular scientific challenge, since it is difficult to precisely monitor mineralization processes *in situ*. We have recently

presented a new approach that enables the correlative application of a range of characterization techniques to closely monitor crystallization processes within hydrogels.[26] Here we apply this toolbox to study the formation and transformation of CaP-mineral within an alginate matrix at low pH (approx. pH 5) and the influence of brushite seeds dispersed in the matrix under otherwise identical conditions. The non-destructive characterization techniques were also used to monitor the transformation behavior of minerals within alginate hydrogels during incubation in simulated body fluid (SBF), providing a means to measure the same samples over several time points. This resulted in a thorough spatiotemporal description of the gel and mineral formation, maturation and transformation pathways at the microscale in unprecedented detail.

## 2. Experimental

### 2.1. Flow cell samples

De-ionized water (DIW, with a resistivity of 10-15 M $\Omega$ cm) was used in all of the experiments. Alginate solutions were prepared with 1.8 mass% alginate ( $M_W=2.74 \times 10^5$  g mol $^{-1}$ ,  $F_G=0.68$ , FMC Biopolymer, Norway), 0.9 mass% NaCl (VWR, Pennsylvania, USA) and a mixture of Na $_2$ HPO $_4 \cdot 7$  H $_2$ O (Thermo Fisher Scientific, Norway) and NaH $_2$ PO $_4 \cdot 2$  H $_2$ O (Sigma Aldrich, Norway) to a phosphate concentration of 100 mM or 300 mM with pH 7. A 1.5  $\mu$ L droplet of alginate solution was placed between two glass slides separated by 140  $\mu$ m in order to produce a disc. A 1 M CaCl $_2$  (Sigma Aldrich, Norway) solution buffered either at pH 5 with sodium acetate (NaAc) (Sigma Aldrich, Norway) or at pH 7 with Tris(hydroxymethyl)aminomethane (TRIS) (Sigma Aldrich, Norway) was introduced into the flow cell initiating the gelling and mineralization process as the calcium diffused into the disc. SBF was made according to Kokubo *et al.*[27] Samples were placed in 50 mL of SBF and the solution was replenished with fresh SBF every 24 h.

## 2.2. Preparation of crystals for seeding and Raman analysis

80 Brushite seed crystals were made by mixing 500 mL of 0.4 M  $\text{Ca}(\text{NO}_3)_2 \cdot 4\text{H}_2\text{O}$  (Sigma Aldrich, Norway) and 500 mL of 0.4 M  $\text{KH}_2\text{PO}_4$  (Sigma Aldrich, Norway) and 26 mM KOH (Sigma Aldrich, Norway). The resulting precipitate was aged for 2 h before they were washed and filtered with DIW and ethanol. The size of the crystals was measured using a Coulter Counter Multisizer 3  
85 (Beckman Coulter, California, USA). The seed crystals were ground using an agate pestle and mortar in order to disrupt any aggregation and 0.2 mass% were added to alginate solutions under stirring. The solutions were left stirring for 1 h to ensure uniform distribution of the seed crystals.

OCP and HAp were made according to methods described by Elliott.[28]  
90 Briefly, OCP was made by hydrolyzing brushite crystals in 0.5 M NaAc (pH>9) at 37 °C for 1 week. The solution was replenished daily. HAp was made by slowly dripping a solution with 640 mM  $\text{Ca}(\text{NO}_3)_2$  into an equal volume of 250 mM  $(\text{NH}_4)_2\text{HPO}_4$  (Sigma Aldrich, Norway) under rapid stirring. Both solutions had an initial pH above 10 and  $\text{NH}_4\text{OH}$  (Sigma Aldrich, Norway) was used to  
95 maintain pH above 10. The resulting precipitate was aged over night.

The resulting crystals were in all cases washed and filtered using DIW and ethanol and phase purity was measured using powder XRD (D8 Advance DaVinci, Bruker AXS GmbH, Germany) prior to Raman measurements, see Figures S.1, S2 and S3 in the Supplementary Information.

## 100 2.3. Characterization

Dark-field and phase contrast images of alginate samples with varying phosphate content, see Table 1, were recorded using an optical microscope (Nikon Eclipse TS100) through a 4 X lens at 4 FPS for the first 15 s and at 0.2 FPS during the remaining gelation process. The images were analyzed with MATLAB  
105 (2014b) in order to extract the velocity at which the gel front moved, briefly a series of images of the moving gel front was recorded and the position of the front was fitted with an ellipse. A gel front radius was calculated by averaging the two ellipse axis (in all cases the shape was close to circular) and the position

of the front was plotted as a function of time. The linear region of the resulting  
110 plot was used to calculate the gel front velocity, cf. Figure S.4. Further details  
of the analysis are given elsewhere.[26]

Selected samples were critical point dried (Emitech K850 critical point dryer),  
mounted on aluminum stubs using carbon tape and coated with 3-5 nm plat-  
inum/palladium (Cressington 208 HR) before SEM-analysis (Hitachi S-5500).

115 Raman microspectroscopy (Renishaw InVia Reflex) was performed by mak-  
ing 120 measurements (integration time 1 s, 30 accumulations) at one spot  
directly after the gelling solution had been introduced. Line scans consisting of  
recorded spectra (integration time 1 s, 30 accumulations) from 50 points along  
the radius of mineralized alginate discs were also collected 1 h and 24 h after the  
120 gelling solution had been introduced. All measurements were performed with a  
535 nm laser through a 10 X lens. Confocality was reduced at the expense of  
spatial resolution in order to obtain an average signal from the whole thickness  
of the disc.

By adding 20  $\mu\text{M}$  R6G-EDA (rhodamine 6G modified with ethylenediamine  
125 according to published methods[29, 30]) and 5  $\mu\text{M}$  sulforhodamine 101 (SR101,  
Sigma Aldrich, Norway) pH measurements were performed using confocal laser  
scanning microscopy (Leica TCS SP5). Images were recorded at 0.1 FPS for  
a duration of 33 min. Details of the measurements settings and analysis are  
presented elsewhere.[26] Briefly, the intensity ratio between a pH-sensitive and  
130 pH-insensitive dye was compared to a standard curve made using the same  
measurement conditions in order to calculate the pH in each pixel of the images.

### 3. Results and discussion

Previously we have shown that the velocity of the alginate gel front was lim-  
ited by inwards diffusion of  $\text{Ca}^{2+}$ . [26] Tanaka *et al.* has shown that the diffusion  
135 of molecules with a molecular weight lower than  $2 \times 10^4$  is the same in water,  
as it is in gels made with 2 % or 4 % alginate, indicating that viscosity does  
not affect the diffusion of small molecules in this system.[31] With the addition

of phosphate to this system, there is a simultaneous consumption of calcium ions due to precipitation of a mineral phase within the gel network. Therefore  
 140 it follows that the gel front velocity is likely to reduce. To investigate this experimentally we studied the gel front evolution in our flow cell with additional phosphate present in the hydrogel phase using optical microscopy. Figure 1 a-c shows a typical phosphate containing sample during the gelation process. Due to a difference in refractive indexes between gelled and ungelled alginate, the  
 145 position of the gel front was clearly visible in phase contrast microscopy, see Figure 1 a. Using dark field microscopy, the mineralized gel was clearly visible due to the fact that it scattered more of the incoming illumination, seen in Figure 1 b and c. Figure 1 d shows a bar plot of the gel front velocity for the different samples.

Table 1: An overview of the composition of the different alginate samples studied. Alginate concentration was in all cases 1.8 mass%. AlgP0 and AlgP0DCPD were not buffered.

Sample	Phosphate conc. [mM]	Initial pH	DCPD seed conc. [mass%]
AlgP0	0	~7	-
AlgP100	100	7	-
AlgP300	300	7	-
AlgP0DCPD	0	~7	0.2
AlgP300DCPD	300	7	0.2

150 As expected, the gel front velocity was greatest for phosphate free samples and decreased with increasing phosphate concentration. Table 1 provides a summary of the conditions used for the different samples. An interesting characteristic of the mineralization process was observed in dark field microscopy: the leading edge of the mineralization zone contained a narrow region which  
 155 scattered more light, indicated by asterisks in Figure 1 b and c. This region, appearing as a brighter band, moved inwards immediately behind the gel front as the mineralization progressed and it is formed at the same time or just after

influx of the Ca-ions and the resulting gelling of alginate (cf. Figure 1 b and c). This change of position indicated that the origin of this region was a metastable  
160 phase which transformed or dissolved after a relatively short time ( $\sim 120$  s as estimated from the images). The nature of this phase is investigated in details below. In this geometry, supersaturation with respect to CaP was highest close to the gel front and would be quickly reduced once the mineral phase had formed. It is therefore likely that this transient zone was located close to the  
165 region with the highest supersaturation, and contained a metastable form of CaP.

We have previously shown the potent effect of brushite seed crystals on phase selection within alginate hydrogels and with the added benefit of our spatiotemporal characterization toolbox we further investigate this effect here.[15] It has  
170 previously been shown that alginate, and especially the guluronate residues (G-blocks) which have a high affinity for calcium, have an inhibitory effect on the nucleation (and growth) of calcium phosphate crystals.[16]. Chelation of calcium ions is a likely explanation for the nucleation inhibition, while non-specific interactions between alginate and crystals and specific interactions between G-  
175 blocks and active growth sites are probable causes of growth inhibition. Considering this inhibitory effect of alginate on the nucleation (and growth) of calcium phosphate, as observed by us and others, we expected that the addition of seed crystals would increase the  $\text{Ca}^{2+}$  consumption rate, as it would not rely on nucleation of new crystals.[16, 32] We tested this hypothesis by incorporating 0.2  
180 mass% brushite seed crystals with an average size of  $30 \mu\text{m}$  in alginate containing 300 mM phosphate precursor and monitored gel front velocity and crystal growth. For these samples, one might expect the gel front velocity to be reduced to a larger extent compared to samples without seed crystals, due to an increased consumption of  $\text{Ca}^{2+}$ . However, no significant difference was observed  
185 experimentally (Figure 1 d). A transient zone similar to the one observed for unseeded samples was also observed close to the mineral front for seeded samples, see Figure 2. These observations indicate that a similar process was responsible for the initial reduction in the calcium and phosphate concentrations for both

seeded and unseeded samples. For brevity, we term the three observed regions  
190 ungelled, transient and gelled; however, note that the transient zone has also  
been crosslinked and is to be considered a gelled region. Details of this trans-  
formation process focusing on phase composition, transformation kinetics and  
morphology of the formed mineral phases are described below.

To characterize the phase composition of the mineral formed in the experi-  
195 ments described above in real time, we used confocal Raman micro-spectroscopy  
(CRM) since this technique allows both spatial and temporal resolution of small  
sample volumes (typical sample volume was 1.5  $\mu\text{L}$ ) without recourse to dehy-  
drate the sample. Initially, Raman spectra were collected from an area approx-  
imately 200  $\mu\text{m}$  from the edge of the sample, as indicated in Figure 2. 120  
200 scans were recorded consecutively for one hour from the same location following  
the introduction of  $\text{Ca}^{2+}$  to allow observation of mineral evolution. Figure 3 a  
shows Raman spectra of an AlgP300 sample at the indicated time points. These  
spectra have not been normalized, and are scaled according to the measurement  
time. The spectrum denoted 0 s was recorded from the alginate droplet be-  
205 fore the calcium solution had been introduced and contains four main peaks:  
the three peaks with highest intensity originate from the phosphate ions in the  
solution. The peaks at  $879\text{ cm}^{-1}$  and  $1078\text{ cm}^{-1}$  were assigned to symmetric  
stretching of P-(OH)<sub>2</sub> and P-O<sub>2</sub> respectively for  $\text{H}_2\text{PO}_4^-$ , while the peak at  $990\text{ cm}^{-1}$   
was due to symmetric stretching of P-O<sub>3</sub> in  $\text{HPO}_4^{2-}$ . [33] The weaker P-  
210 OH stretching from this ion was found by curve fitting at  $852\text{ cm}^{-1}$  overlapping  
with the  $879\text{ cm}^{-1}$  peak from  $\text{H}_2\text{PO}_4^-$ . The weak peak located around  $810\text{-}816\text{ cm}^{-1}$   
was assigned to the alginate polymer. [34] Alginate also has a peak located  
at  $890\text{-}892\text{ cm}^{-1}$ , which overlaps with one of the  $\text{H}_2\text{PO}_4^-$  peaks and could not  
be resolved. As calcium was introduced the  $\text{HPO}_4^{2-}$  peak intensity was quickly  
215 reduced, while the  $\text{H}_2\text{PO}_4^-$  peak intensities were gradually reduced. We note  
that the transient zone did not give any strong Raman signal. However, a weak  
and broad peak located at  $955\text{ cm}^{-1}$  which, over time, split into two overlapping  
peaks located at  $946\text{ cm}^{-1}$  and  $957\text{ cm}^{-1}$  was observed. The intensity of the  $946\text{ cm}^{-1}$   
peak was reduced while the  $957\text{ cm}^{-1}$  peak increased in intensity, became

220 sharper and shifted towards higher wavenumbers as time progressed, as shown  
in Figure 3 a. The appearance and reduction in intensity of this broad peak cor-  
responded to the appearance and disappearance of the transient region observed  
in optical microscopy. Peak sharpening is indicative of increased crystallinity  
and the observed peak shift is indicative of mineral maturation similar to that  
225 which was previously observed in a bone tissue model.[10] Different literature  
sources report the Raman signal from amorphous calcium phosphate ACP to  
be a broad peak centered at 945-955  $\text{cm}^{-1}$ . [9, 10, 35] Although the signal was  
weak, this was interpreted as an indication that the mineral in the transient  
region was amorphous. After 15 min a peak appeared around 928-935 which  
230 was assigned to the C-C stretching of acetate, which was due to the buffer dif-  
fusing into the hydrogel.[36] The same measurements were repeated on a similar  
sample infused with a TRIS-buffered  $\text{Ca}^{2+}$  solution at pH 7. The same weak  
ACP peak at 955  $\text{cm}^{-1}$  was observed here without the interfering acetate peak  
at 932  $\text{cm}^{-1}$ , see Supplementary Information Figure S.5 b.

235 After 1 h, a line scan consisting of 50 points from the edge of the disc towards  
the center was recorded in order to investigate any spatial differences along the  
radius. The line scan was repeated over the same area after 24 h in the mother  
liquor. Figure 3 c and d show Raman spectra recorded from three such points  
in an AlgP300 sample after 1 h and 24 h, respectively. The position of the  
240 spectra are given as a distance from the center. The phosphate in CaP-phases  
such as brushite, HA and TCP have easily distinguishable Raman spectra.[37]  
However, it is more challenging to differentiate between HA and OCP. Crane  
*et al.* used a weak peak, arising from  $\nu_1$   $\text{HPO}_4$  stretching, positioned around  
1010  $\text{cm}^{-1}$  to identify OCP.[10] As a result of the experimental design in this  
245 work, the 1010  $\text{cm}^{-1}$  peak was almost at the same level as the background noise  
(cf. Supplementary Information Figure S.5 a), and was not deemed suitable.  
Instead the peak shape and position of the main phosphate peak was used to  
determine the dominating phase. Fowler *et al.* have thoroughly assigned the  
different Raman bands of OCP and show a main peak situated around 956-  
250 959  $\text{cm}^{-1}$  with a strong shoulder at 966-967  $\text{cm}^{-1}$ , both arising from  $\nu_1$   $\text{PO}_4$

stretching.[38] The  $\nu_1$  PO<sub>4</sub> stretching of HAp is reported to be a single peak located at 959-962 cm<sup>-1</sup> with a weak and broad shoulder at around 950 cm<sup>-1</sup> leading to an asymmetric peak shape of the main phosphate peak of HAp.[39] The difference in peak shape between OCP and HAp are clearly visible in the spectra of pure phase samples shown in Figure 3 b. Therefore, fitting of the recorded spectra in a region between 920 and 980 cm<sup>-1</sup> was used to determine the dominating crystal phase, shown in red (OCP) and blue (HAp) in Figure 4. Figure 4 a and b show micrographs of an AlgP300 sample after 1 h and 24 h incubation in the mother liquor. The line scans from the sample are visualized in Figure 4 c and d, where the intensity of the peak located at 958 cm<sup>-1</sup> (the main phosphate peak in the spectra arising from  $\nu_1$  PO<sub>4</sub> stretching[37]) has been plotted as a function of distance from the center for the two samples. The intensity at 987 cm<sup>-1</sup>, corresponding to the main peak of brushite has also been plotted. The lines mark the position of the CRM line scans and the numbers refer to the position of SEM-images shown in Figure 7. It was found that the mineral present in the hydrogel after 1h was mainly OCP, although a narrow band towards the edge of the disc was predominantly HAp, see Figure 4 c. After storage for 24 h in the gelling solution, a more heavily mineralized band was seen in optical microscopy along the edge of the disc, see Figure 4 b. The Raman intensity in the outer region of the disc and the width of the HAp dominated region had both increased compared to the 1h sample, as shown in Figure 4 d. No brushite was observed within the alginate network in these experiments, the small rise in the black curve is due to background noise .

The same set of CRM measurements was repeated for samples containing 0.2 mass% brushite seeds mixed into the alginate solution with 300 mM phosphate, denoted AlgP300DCPD. A weak broad peak located at 955 cm<sup>-1</sup> was also seen for these samples, however instead of shifting towards higher wavenumbers, it disappeared as the brushite peak at 987 cm<sup>-1</sup> increased in intensity, as seen in the inset of Figure 5 a. The initial peak at 955 cm<sup>-1</sup> was present for less than a minute, which corresponds to the appearance of the transient region observed by optical microscopy. Figure 5 b shows the Raman spectrum for a

pure phase brushite sample. After 1 h and 24 h, line scans were performed. Three spectra from chosen positions at both time points are shown in Figure 5 c and d. Micrographs of this sample after 1 h and 24 h incubation in the mother liquor are shown in Figure 6 a and b. The intensity at  $960\text{ cm}^{-1}$  and  $987\text{ cm}^{-1}$  have been plotted as a function of distance from the center in Figure 6 c and d. In contrast to the line scan for unseeded samples, which was relatively smooth with the Raman signal intensity highest at the edge of the disc and gradually decreasing towards the center, the seeded samples resulted in a more jagged signal which persisted into the center of the disc. This was interpreted as a result of the larger brushite crystals present in the hydrogel. These crystals were larger than the laser beam spot size and more dispersed within the hydrogel network. As a result the Raman signal originating from the mineral crystals appear more discrete along the line scan for the AlgP300DCPD samples. For the AlgP300 samples, the crystals were much smaller than the spot size and a more averaged signal from both mineral and hydrogel was obtained in every point spectrum. Both optical images and CRM measurements indicated that there was less mineral towards the center, but nevertheless growth of the seeds occurred throughout the sample. A micrograph of the sample before  $\text{CaCl}_2$  was introduced can be seen in the Supplementary Information (Figure S.6). A line scan was repeated in the same area following 24 h incubation in the mother liquor, seen in Figure 6 d. The brushite peak at  $987\text{ cm}^{-1}$  disappeared towards the edge of the disc and was replaced by a peak located at  $960\text{ cm}^{-1}$ , indicating conversion of brushite to HAp. There was no evidence in the Raman data that OCP was part of the transformation pathway when brushite had precipitated first.

To determine the crystal morphology and distribution of the mineral within the hydrogel network, selected samples were prepared for SEM-analysis. Figure 7 shows images recorded for an AlgP300 sample kept in the gelling solution for 1 h (a, b and c) and for 24 h (d, e and f). Their corresponding positions (1=a, 2=b etc.) are shown in Figure 4. Figure 7 a shows an image recorded from the center of a disc. No mineral could be seen in this area corroborating

the CRM and optical microscopy results. The images in Figure 7 b and c show a combination of nodules intertwined with alginate fibers (black arrowheads) and flaky plate-like crystals (white arrowheads). These crystals were more numerous in Figure 7 c which was recorded at a position closer to the edge of the disc. Following storage for 24 h in the gelling solution, mineral located in the same region as Figure 7 b had grown considerably and appeared more plate like (Figure 7 d). The Raman signal from the same region did not increase in intensity and showed no sign of peak sharpening which indicates that the amount of mineral or degree of crystallinity did not change. The larger crystals seen in Figure 7 d as compared to Figure 7 b are then likely the result of Ostwald ripening, where larger crystals have grown at the expense of smaller crystals without changing the total amount of mineral within this region. Peak fitting of the OCP dual-peak revealed that the center of the two peaks was shifted from 957 to 958  $\text{cm}^{-1}$  and 965 to 966  $\text{cm}^{-1}$ , respectively. The exact origin of this shift is not known, however it could be a similar maturation process as previously described for HAp.[10] The images in Figure 7 e and f, show an abundance of well formed crystals. Within the hydrogel, large platelets with feathered edges were found (Figure 7 e), contrasting to well defined acicular crystals at the outermost region of the disc (Figure 7 f). See Figure S.7 in the Supplementary Information which shows a lower magnification overview to confirm the uniform mineral distribution over the different regions. Raman spectra from these regions revealed that the mineral in Figure 7 b, c and d was OCP while the mineral in e and f was HAp.

Figure 8 shows an AlgP300DCPD sample prepared at pH 5 and kept in the gelling solution for 1 h (a, b and c) and 24 h (d, e and f). For samples stored for 1 h, large brushite crystals were observed throughout the alginate matrix, as shown in Figure 8 a and b. The size of these brushite crystals, and the absence of smaller crystals, indicated that nucleation of new crystals did not occur within the hydrogel network. This was further supported by observations described below, where the mineralization process was visualized immediately after precipitation of the mineral phase. No evidence of small brushite crystals

was found and dissolution of ACP which was consumed by growth of brushite  
345 seeds was observed (cf. Figure 9 e). In addition, a dense layer of crystals on  
the outer surface of the disc was also present. This layer, shown in Figure 8 c  
was probably a result of the high supersaturation in this region, in combination  
with uninhibited growth into the surrounding solution. After 24 h, this surface  
layer was not present and the crystal structure close to the surface of the disc  
350 had changed from large brushite platelets to acicular HAp crystals similar to  
those observed in the same region of the AlgP300 samples, (cf. Figure 8 f and  
Figure 7 f). This sample fractured during mounting and the surface to the left  
in Figure 8 d shows a cross-section of the disc. A magnified image of this section,  
shown in Figure 8 e, reveals that the crystals were also needle-like further into  
355 the alginate network in contrast to unseeded samples which had platelets in the  
same region. This also confirms that the crystals were present throughout the  
thickness of the disc. CRM analysis of this region showed that these crystals  
were HAp.

Both optical microscopy and CRM showed that a metastable phase was  
360 present in the early stages of mineralization in the alginate discs. Based on  
observations from optical microscopy we estimate that, once formed, this phase  
was stable for no more than 120 s. In order to study the morphology of this  
phase, samples were kept in the gelling solution until the gel formed approxi-  
mately halfway through the disc, after which they were flushed with DIW. This  
365 was immediately followed by opening the flow cells and plunging the hydrogel  
discs into 96 % ethanol in order to prevent any dissolution or transformation of  
precipitated CaP phases. The samples were exposed to the gelling solution for  
approximately 3 min, leaving three distinct regions corresponding to the regions  
shown in Figure 2. Figure 9 a-c show an AlgP300 sample prepared at pH 5 and  
370 arrested after 3 min reaction time. In the overview image (Figure 9 a) the gelled  
region, transient region and ungelled region are marked with the same colors  
as in Figure 2. The image in Figure 9 b was recorded within the gelled region,  
nodules and flaky crystals similar to the ones observed for 1 h samples were  
present (cf. Figure 7 b). The transient region, shown in Figure 9 c contained

375 spherical particles with a size range between 30 and 400 nm. These particles  
were uniformly distributed within the alginate network. Several nodules, inti-  
mately connected with alginate fibers, were also observed in this region. These  
nodules were larger and less numerous than the spherical particles which sug-  
gests that the transformation of the spherical particles into nodules and later  
380 flaky platelets is solution based and not a solid state transformation.

Figure 9 d-f show an AlgP300DCPD sample prepared at pH 5 and arrested  
after 3 minutes reaction time. Spherical particles were also observed for this  
sample in the transient zone (marked white in Figure 9 d). Figure 9 e shows  
a brushite seed crystal located in the transient zone. The spherical particles  
385 were not observed in the immediate vicinity of this seed, shown at higher mag-  
nification in Figure 9 f. In the gelled region, (marked blue in Figure 9 d), no  
spherical particles were observed and an abundance of brushite crystals (size  
range 20 to 80  $\mu\text{m}$ ) could be seen within the hydrogel, similar to those ob-  
served by optical microscopy. The absence of spherical particles in the gelled  
390 region, and the consumption of these particles around the brushite seeds indi-  
cated that they consisted of a metastable phase which appeared to reprecipitate  
into growing DCPD crystals. This is consistent with CRM observations. The  
SEM observations are strong indications that this transformation happens via  
a dissolution-recrystallization process.

395 Figure 9 g-i show magnified images of spherical particles found in the tran-  
sient region of an AlgP300DCPD sample prepared at pH 5 (g), an AlgP300  
sample prepared at pH 5 (h) and an AlgP300 sample prepared at pH 7 (i).  
The spherical particles had a non-uniform diameter ranging from 30 to 400 nm  
and appeared identical regardless of the initial conditions in which they were  
400 made. Elliott reports that ACP is often present as spherical particles in the  
range of 20-120 nm, which fits well with our conclusion that these particles are  
ACP.[28] The SEM analysis in combination with CRM suggests that ACP was  
formed initially which then rapidly transformed into OCP or HAp for unseeded  
samples and into brushite for samples seeded with brushite crystals. In both  
405 cases transformation into the more stable HAp phase occurred gradually and all

transformations were likely to have taken place via a dissolution-precipitation process.

pH is an important factor in determining nucleation and growth of different CaP-phases.[40] In solution, ions diffuse readily and the pH can be expected to  
410 be uniform throughout the sample volume. The situation was somewhat more complex within the system studied in this work. The alginate was initially buffered at pH 7, and the gelling solution was buffered at pH 5 or pH 7 and as CaP precipitated,  $H^+$  was released locally. In order to gain information regarding the dynamics of the pH in the system, optical measurements with a  
415 pH-sensitive dye were performed. We have previously shown this method to be highly sensitive to changes in pH between 4 and 6.5.[26] Figure 10 a shows the pH value for three different samples averaged from a 121 x 121  $\mu m$  area in the center of the alginate discs as a function of time from when the gelling solution was introduced. The measurements show a local generation of  $H^+$   
420 at the mineralization front which consequently diffused inwards to the center of the disc and outwards into the surrounding solution. This can be seen in Figure 10 b and c where a reduction in pH was observed both in the center of the discs and in the surrounding solution. In the sample subjected to a calcium solution of pH 5, part of the decrease in pH is due to the inwards diffusion of  
425 the acidic calcium solution. However, the similarity in the shape of the curves in Figure 10 a indicate that the generation of  $H^+$  is the main reason for the change in pH regardless of the initial pH in the gelling solution. In addition, careful examination of the curve denoted AlgP300 pH5 edge in Figure 10 b reveals a slight u-shape. This u-shape is more clear in Figure 10 c, where both  
430 the alginate solution and the calcium solution was initially pH 7. In this case, the only source of  $H^+$  was the precipitation of CaP. This shape indicates the outward diffusion of  $H^+$  generated from the mineral formation. It can be seen that the surrounding calcium solution experienced a reduction in pH as the local generation of  $H^+$  exceeded the buffering capacity. A subsequent increase in pH  
435 occurred as the solution regained its buffering capacity due to its comparatively larger volume. In both cases the pH in the center and at the halfway point are

expected, with time, to reach the same pH-value of the surrounding solution.

As seen in Figure 10 a, the pH in the center of the discs changed most within 150-350 s after the introduction of the gelling solution. The results from the SEM and CRM analysis show that ACP is the dominant mineral phase within this time frame. This suggests that formation of ACP is the main cause of H<sup>+</sup> release. The subsequent transformation into OCP or brushite appear to have occurred under similar conditions, i.e. pH < 5, for all sample types as can be seen from the similar shape of the curves in Figure 10 a. In cases where brushite seeds were present, the amorphous phase was then consumed due to growth of brushite crystals, likely via a dissolution-reprecipitation pathway. For unseeded samples, consumption of the amorphous phase occurred via nucleation and growth of OCP at the same pH-conditions as for the seeded samples. It is likely that the alginate inhibited the nucleation of brushite, as one would expect this phase to nucleate at a pH-value less than 5.[16, 40] As some of the phosphate was consumed in the mineralization process, the buffering capacity of the alginate solution was reduced. Due to the local generation and fast diffusion of H<sup>+</sup>, the central region of the disc experienced the lowest recorded pH, as can be observed in Figure 10 b and c. Due to a lower concentration of buffer in the surrounding solution, the diffusion of the buffer was slower than the mineral front, leading to a prolonged duration of reduced pH in the center of the discs, see Figure S.10 in the Supplementary Information for a brief discussion of this effect. We speculate that not only the consumption of the available phosphate in the sample, but also a reduction in pH led to the unmineralized zone in the center of gelled discs. This is because pH is an effective variable on supersaturation and reduced pH would lead to lower supersaturation which in turn results in reduced nucleation of new crystals. This may also explain why in seeded samples crystals grew throughout the geometry (cf. Figure 6 and Figure S.9) since this process was not dependent on nucleation.

Incubating materials in simulated body fluid (SBF) has previously been used to indicate the ability of samples to nucleate HAp in physiological conditions.[27] The relevance of this incubation to predict *in vivo* behavior is a matter of

debate.[41] In particular, there have been investigations with both false positives and false negatives, leaving no definitive trend.[42] However, the method  
470 is also often used to form an apatite layer on synthetic scaffold which is believed to enhance the bone bonding ability of the implant.[2, 21, 43–45] In this work, it was used to study how the incorporation of CaP in the alginate matrix affected the formation of HAp, and demonstrate the ability to monitor this transformation with spatiotemporal resolution, not to predict an *in vivo*  
475 response. AlgP300DCPD samples were examined with CRM (shown in Supplementary Information, Figure S.9) and SEM as prepared (Figure 11 a-c) and following 24 h (Figure 11 d-f) and 168 h (Figure 11 g-i) incubation in SBF. As a control, alginate samples which contained brushite seeds, but no phosphate precursor, were also incubated and analyzed with CRM. For the mineralized  
480 samples, a large number of brushite crystals were observed to be protruding out from the hydrogel surface initially, as shown in Figure 11 a. Figure 11 b shows a region close to the edge of the sample where a shell of large brushite crystals could be observed along the edge and individual crystals were also observed embedded in the alginate network. Figure 11 c shows brushite crystals  
485 from a region nearer the center of the disc, revealing that large crystals were also present in this region, in contrast to the unseeded samples (cf. Figure 7 a). Following 24 h incubation in SBF there was a reduction in the abundance of large brushite crystals in all areas of the sample (Figure 11 d). A dense band of small plate like aggregated crystals had formed from the edge and 100-200  
490  $\mu\text{m}$  towards the center of the disc (Figure 11 e). As shown in Figure 11 f, some of the individual brushite crystals had these new crystals encrusted directly on their surfaces. The new crystalline phase was confirmed to be HAp with CRM (see Figure S.9 in Supplementary Information). The dense layer of brushite crystals at the periphery of the sample had completely transformed into HAp,  
495 however the micro scale morphology of these crystals was still intact (see Figure S.8). Following one week storage in SBF, all of the large brushite crystals within the alginate network had dissolved (Figure 11 g) and a dense shell of HAp had formed along the edge of the disc (Figure 11 h). This shell extended ca. 200

$\mu\text{m}$  towards the center of the disc (Figure 11 i), and the alginate network was  
500 heavily mineralized throughout the thickness of the disc (observed from sam-  
ples which fractured during preparation). Figure 11 h and i clearly demonstrate  
that HAp formed uniformly along the edge of the disc and non-uniformly at  
the location of brushite crystals further into the disc. This indicated that the  
source of HAp formation was driven by both dissolution of brushite crystals  
505 and inwards diffusion of the SBF-solution along the edge while further into the  
disc, the primary source for HAp nucleation and growth was the dissolution  
of the resident brushite crystals. The non-mineralized control samples did not  
show any HAp formation within the alginate network, however after 1 week of  
incubation, some HAp had formed on the interface between the hydrogel and  
510 the surrounding solution (see Figure S.9). This shows that the mineralized hy-  
drogel promotes the formation of HAp at physiological pH, probably due to an  
increased, localized supersaturation provided by the dissolution of brushite.

#### 4. Conclusion

In summary, we have shown that by combining a simple experimental design  
515 with several correlative advanced characterization techniques, new insight into  
the mineralization processes within hydrogels can be obtained. Simultaneous  
gelling and mineralization of an alginate hydrogel was performed and spatiotem-  
porally monitored using a thin disc geometry that was particularly convenient  
for optical based *in situ* characterization techniques. It was found that at high  
520 concentrations of mineral precursor, a metastable ACP phase initially formed.  
At pH 5 this phase transformed quickly (within 120 s) into OCP and subse-  
quently (over the course of tens of hours) into HAp. This transformation path  
was altered by introducing crystal seeds in the hydrogel matrix. Brushite seeds  
induced the growth of brushite instead of OCP which later transformed into the  
525 more thermodynamically stable HAp. Transformation of brushite into HAp fol-  
lowing incubation in SBF was also monitored, thereby demonstrating utility of  
this characterization toolbox for non-destructive *in situ* evaluation of hydrogel

based hard tissue scaffold biomaterials.

## 5. Acknowledgments

530 The authors thank the Research Council of Norway for financial support  
(FRINATEK project 214607).

## References

- [1] S. Van Vlierberghe, P. Dubruel, E. Schacht, Biopolymer-based hydrogels as scaffolds for tissue engineering applications: A review, *Biomacromolecules* 12 (5) (2011) 1387–1408.  
535
- [2] K. Gkioni, S. C. Leeuwenburgh, T. E. Douglas, A. G. Mikos, J. A. Jansen, Mineralization of hydrogels for bone regeneration, *Tissue Engineering Part B: Reviews* 16 (6) (2010) 577–585.
- [3] A. K. Gaharwar, N. A. Peppas, A. Khademhosseini, Nanocomposite hydrogels for biomedical applications, *Biotechnology and Bioengineering* 111 (3) (2014) 441–453, [arXiv:NIHMS150003](https://arxiv.org/abs/150003).  
540
- [4] H.-R. Lin, Y.-J. Yeh, Porous alginate/hydroxyapatite composite scaffolds for bone tissue engineering: preparation, characterization, and in vitro studies., *J Biomed Mater Res B Appl Biomater.* 71 (1) (2004) 52–65.
- [5] M. Rajkumar, N. Meenakshisundaram, V. Rajendran, Development of nanocomposites based on hydroxyapatite/sodium alginate: Synthesis and characterisation, *Materials Characterization* 62 (5) (2011) 469–479.  
545
- [6] Z. Li, Y. Su, B. Xie, H. Wang, T. Wen, C. He, H. Shen, D. Wu, D. Wang, A tough hydrogelhydroxyapatite bone-like composite fabricated in situ by the electrophoresis approach, *Journal of Materials Chemistry B* 1 (12) (2013) 1755.  
550

- [7] M. S. Johnsson, G. H. Nancollas, The Role of Brushite and Octacalcium Phosphate in Apatite Formation, *Critical Reviews in Oral Biology & Medicine* 3 (1) (1992) 61–82.
- 555 [8] R. Boistelle, I. Lopez-Valero, Growth units and nucleation: The case of calcium phosphates, *Journal of Crystal Growth* 102 (3) (1990) 609–617.
- [9] T. Tsuji, K. Onuma, A. Yamamoto, M. Iijima, K. Shiba, Direct transformation from amorphous to crystalline calcium phosphate facilitated by motif-programmed artificial proteins., *Proceedings of the National Academy of Sciences of the United States of America* 105 (44) (2008) 16866–70.
- 560 [10] N. J. Crane, V. Popescu, M. D. Morris, P. Steenhuis, M. a. Ignelzi, Raman spectroscopic evidence for octacalcium phosphate and other transient mineral species deposited during intramembranous mineralization., *Bone* 39 (3) (2006) 434–42.
- 565 [11] G. Campi, a. Ricci, a. Guagliardi, C. Giannini, S. Lagomarsino, R. Cancedda, M. Mastrogiacomo, a. Cedola, Early stage mineralization in tissue engineering mapped by high resolution X-ray microdiffraction., *Acta biomaterialia* 8 (9) (2012) 3411–8.
- [12] J. Mahamid, B. Aichmayer, E. Shimoni, R. Ziblat, C. Li, S. Siegel, O. Paris, P. Fratzl, S. Weiner, L. Addadi, Mapping amorphous calcium phosphate transformation into crystalline mineral from the cell to the bone in zebrafish fin rays., *Proceedings of the National Academy of Sciences of the United States of America* 107 (14) (2010) 6316–6321.
- 570 [13] L. B. Gower, Biomimetic Model Systems for Investigating the Amorphous Precursor Pathway and Its Role in Biomineralization, *Chemical Reviews* 108 (11) (2008) 4551–4627.
- [14] M. Xie, J.-P. Olderøy, Magnus Ø Andreassen, S. M. Selbach, B. L. Strand, P. Sikorski, Alginate-controlled formation of nanoscale calcium carbonate

- and hydroxyapatite mineral phase within hydrogel networks., *Acta biomaterialia* 6 (9) (2010) 3665–3675.
- 580
- [15] S. H. Bjørnøy, D. Bassett, S. Ucar, J.-P. Andreassen, P. Sikorski, Controlled mineralisation and recrystallisation of brushite within alginate hydrogels, *Biomedical Materials* 015013.
- [16] S. Ucar, S. H. Bjørnøy, D. C. Bassett, B. L. Strand, P. Sikorski, J.-P. Andreassen, Nucleation and Growth of Brushite in the Presence of Alginate, *Crystal Growth & Design* (2015) 151005122429007.
- 585
- [17] L. Gower, D. Tirrell, Calcium carbonate films and helices grown in solutions of poly(aspartate), *Journal of Crystal Growth* 191 (1-2) (1998) 153–160.
- [18] H. Cölfen, S. Mann, Higher-order organization by mesoscale self-assembly and transformation of hybrid nanostructures, *Angewandte Chemie - International Edition* 42 (21) (2003) 2350–2365.
- 590
- [19] F. C. Meldrum, H. Colfen, Controlling Mineral Morphologies and Structures in Biological and Synthetic Systems, *Chemical Reviews* 108 (11) (2008) 4332–4432.
- [20] F. Nudelman, K. Pieterse, A. George, P. H. H. Bomans, H. Friedrich, L. J. Brylka, P. A. J. Hilbers, G. de With, N. A. J. M. Sommerdijk, The role of collagen in bone apatite formation in the presence of hydroxyapatite nucleation inhibitors., *Nature materials* 9 (12) (2010) 1004–1009.
- 595
- [21] K. Bleek, A. Taubert, New developments in polymer-controlled, bioinspired calcium phosphate mineralization from aqueous solution., *Acta biomaterialia* 9 (5) (2013) 6283–321.
- 600
- [22] H. Ping, H. Xie, B.-L. Su, Y.-b. Cheng, W. Wang, H. Wang, Y. Wang, J. Zhang, F. Zhang, Z. Fu, Organized intrafibrillar mineralization, directed by a rationally designed multi-functional protein, *J. Mater. Chem. B* 3 (2015) 4496–4502.
- 605

- [23] B. Cantaert, E. Beniash, F. C. Meldrum, Nanoscale confinement controls the crystallization of calcium phosphate: relevance to bone formation, *Chemistry (Weinheim an der Bergstrasse, Germany)* 19 (44) (2013) 14918–14924.
- 610 [24] Y.-W. Wang, H. K. Christenson, F. C. Meldrum, Confinement Increases the Lifetimes of Hydroxyapatite Precursors, *Chemistry of Materials* 26 (20) (2014) 5830–5838.
- [25] A. K. Rajasekharan, M. Andersson, Role of Nanoscale Confinement on Calcium Phosphate Formation at High Supersaturation, *Crystal Growth & Design* 15 (6) (2015) 2775–2780.
- 615 [26] S. H. Bjørnøy, S. Mandaric, D. C. Bassett, A. K. Åslund, J.-P. Andreassen, B. L. Strand, P. Sikorski, Gelling kinetics and mineralization of alginate hydrogels: a correlative spatiotemporal characterization toolbox, Submitted to *Acta Biomaterialia*.
- 620 [27] T. Kokubo, H. Takadama, How useful is SBF in predicting in vivo bone bioactivity?, *Biomaterials* 27 (15) (2006) 2907–15.
- [28] J. Elliott, *Structure and Chemistry of the Apatites and Other Calcium Orthophosphates*, Elsevier B.V., 1994.
- [29] J.-S. Wu, I.-C. Hwang, K. S. Kim, J. S. Kim, Rhodamine-based Hg<sup>2+</sup>-selective chemodosimeter in aqueous solution: fluorescent OFF-ON., *Organic letters* 9 (5) (2007) 907–10.
- 625 [30] Z. Li, S. Wu, J. Han, S. Han, Imaging of intracellular acidic compartments with a sensitive rhodamine based fluorogenic pH sensor., *The Analyst* 136 (2011) 3698–3706.
- 630 [31] H. Tanaka, M. Matsumura, I. a. Veliky, Diffusion characteristics of substrates in Ca-alginate gel beads., *Biotechnology and bioengineering* 26 (1) (1984) 53–58.

- [32] P. Malkaj, E. Pierri, E. Dalas, The crystallization of Hydroxyapatite in the presence of sodium alginate., *J. Mater. Sci: Mater. Med.* 16 (8) (2005) 733–7.
- 635
- [33] W. L. Marshall, G. M. Begun, Raman spectroscopy of aqueous phosphate solutions at temperatures up to 450 C. Two liquid phases, supercritical fluids, and pyro- to ortho-phosphate conversions, *Journal of the Chemical Society, Faraday Transactions 2* 85 (12) (1989) 1963.
- [34] M. M. Campos-Vallette, N. P. Chandía, E. Clavijo, D. Leal, B. Matsuhira, I. O. Osorio-Román, S. Torres, Characterization of sodium alginate and its block fractions by surface-enhanced Raman spectroscopy, *Journal of Raman Spectroscopy* 2009 (August 2009) (2009) n/a–n/a.
- 640
- [35] G. R. Sauer, W. B. Zunic, J. R. Durig, R. E. Wuthier, Fourier transform raman spectroscopy of synthetic and biological calcium phosphates, *Calcified Tissue International* 54 (5) (1994) 414–420.
- 645
- [36] W. W. Rudolph, D. Fischer, G. Irmer, Vibrational spectroscopic studies and DFT calculations on  $\text{NaCH}_3\text{CO}_2(\text{aq})$  and  $\text{CH}_3\text{COOH}(\text{aq})$ , *Dalton Trans.* 43 (8) (2014) 3174–3185.
- [37] S. Koutsopoulos, Synthesis and characterization of hydroxyapatite crystals : A review study on the analytical methods, *Journal of biomedical materials research* 62 (4) (2002) 600–12.
- 650
- [38] B. O. Fowler, M. Markovic, W. E. Brown, Octacalcium phosphate. 3. Infrared and Raman vibrational spectra, *Chemistry of Materials* 5 (10) (1993) 1417–1423.
- 655
- [39] G. Penel, G. Leroy, C. Rey, E. Bres, MicroRaman Spectral Study of the  $\text{PO}_4$  and  $\text{CO}_3$  Vibrational Modes in Synthetic and Biological Apatites, *Calcified Tissue International* 63 (6) (1998) 475–481.

- [40] F. Abbona, H. Madsen, R. Boistelle, The initial phases of calcium and magnesium phosphates precipitated from solutions of high to medium concentrations, *Journal of Crystal Growth* 74 (3) (1986) 581–590.
- [41] M. Bohner, J. Lemaitre, Can bioactivity be tested in vitro with SBF solution?, *Biomaterials* 30 (12) (2009) 2175–9.
- [42] A. A. Zadpoor, Relationship between in vitro apatite-forming ability measured using simulated body fluid and in vivo bioactivity of biomaterials., *Mater Sci Eng C Mater Biol Appl.* 35 (2014) 134–43.
- [43] L. Jongpaiboonkit, T. Franklin-Ford, W. L. Murphy, Growth of hydroxyapatite coatings on biodegradable polymer microspheres., *ACS applied materials & interfaces* 1 (7) (2009) 1504–11.
- [44] I. Hofmann, L. Müller, P. Greil, F. A. Müller, Calcium phosphate nucleation on cellulose fabrics, *Surface and Coatings Technology* 201 (6) (2006) 2392–2398.
- [45] K. Rodríguez, S. Renneckar, P. Gatenholm, Biomimetic calcium phosphate crystal mineralization on electrospun cellulose-based scaffolds., *ACS applied materials & interfaces* 3 (3) (2011) 681–9.

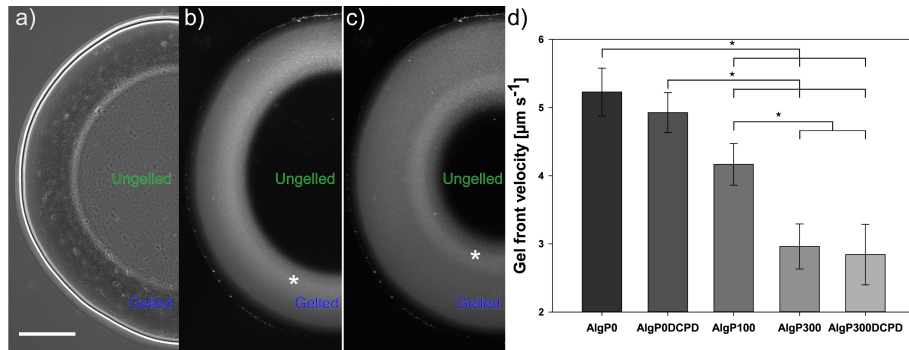


Figure 1: **a**: A phase contrast image of a partially gelled AlgP300 sample. The gel front is clearly visible between the gelled and the ungelled part. Scalebar: 500  $\mu\text{m}$ . **b**: A dark field micrograph showing the gelation and mineralization of an alginate disc after 150 s. **c**: The same sample as in **b** after 300 s. A moving bright band of mineral is marked by an asterisk in **b** and **c**. **d**: Bar plot of the gel front velocity as a function of phosphate concentration and the presence of brushite seeds. The asterisk marks statistically different values (One way ANOVA,  $p < 0.05$ ).

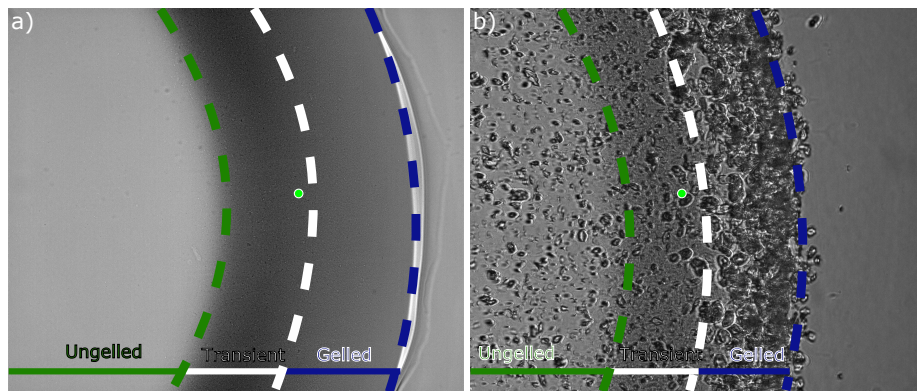


Figure 2: Phase contrast microscopy images showing an AlgP300 (**a**) and an AlgP300DCPD (**b**) sample during the gelling process. Three regions are marked in the images: the ungelled region shown in green, the transient zone shown in white, and a gelled region shown in blue. The marker indicates the approximate position of the CRM time scan. The frame width of the images is 845  $\mu\text{m}$ .

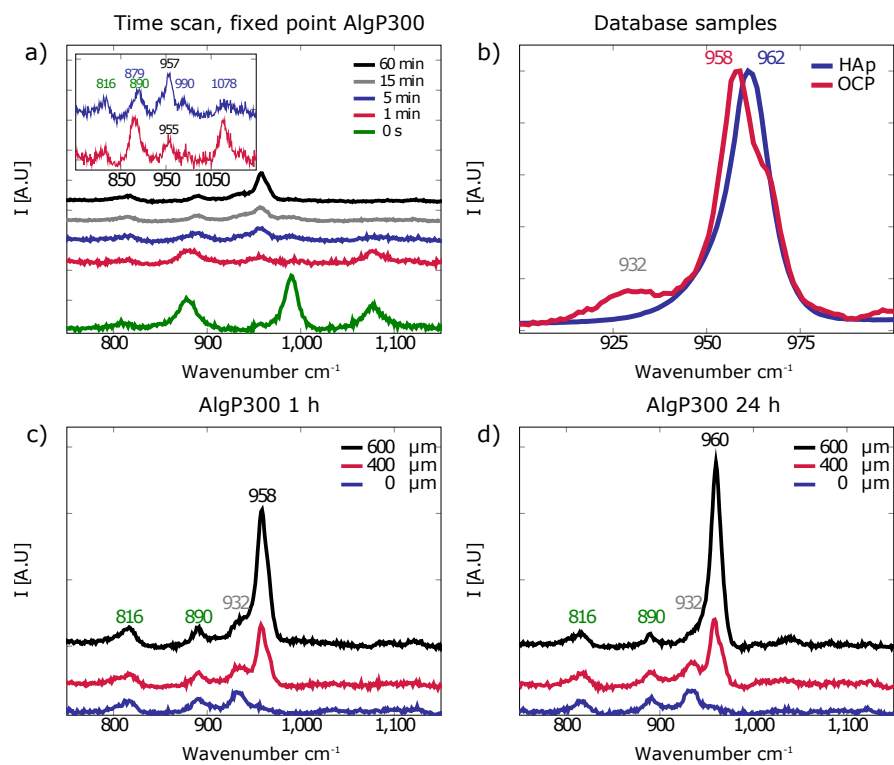


Figure 3: **a)**: Raman spectra of an AlgP300 sample from a single spot at 5 time points. The inset shows the 1 min and 5 min spectra with a reduced y-axis range in order to accentuate the peaks. **b)**: Raman spectra from the main peak of pure phase samples of HAp, and OCP prepared in solution. Note the difference in peak shape between HAp and OCP. **c)** and **d)**: Raman spectra from a line scan of an AlgP300 sample after 1 and 24 h respectively. The spectra names refer to distance from the center of the discs. The numbers in the graph specify peak positions in cm<sup>-1</sup>.

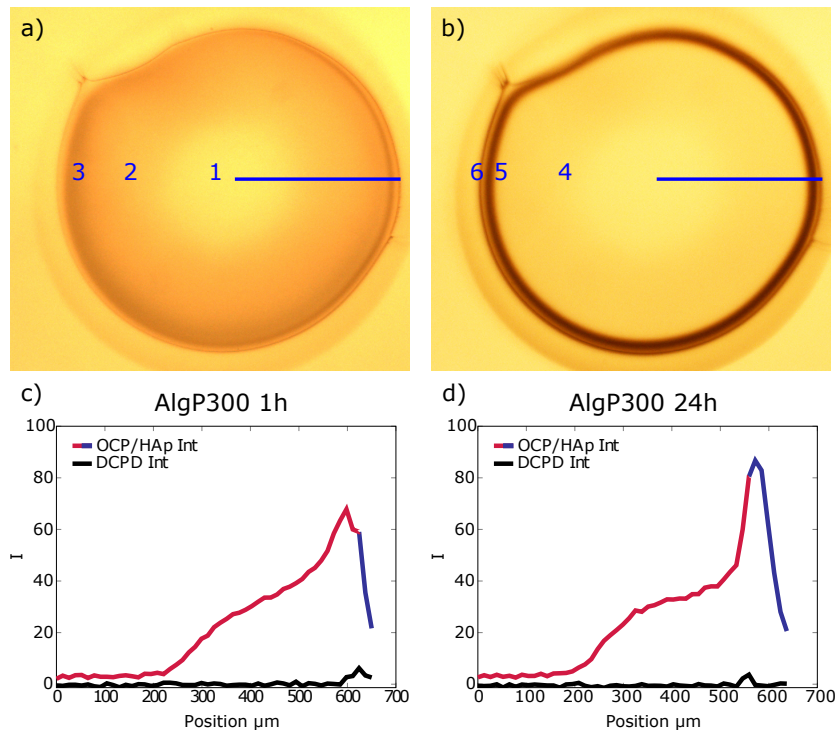


Figure 4: Optical images and Raman data for an unseeded hydrogel disc ( $\varnothing \approx 1.3$  mm) with 300 mM phosphate gelled and mineralized in a 1 M calcium solution at pH 5. **a)** After 1 h in the gelling solution. **b)** After 24 h in the gelling solution. The numbers correspond to positions of the SEM-images shown in Figure 7. **c)** A line scan (shown by the blue line in **a)**) showing the intensity of the  $958\text{ cm}^{-1}$  peak, corresponding to the dominant phase as determined by curve fitting, either OCP in red and HAp in blue. The intensity of the  $987\text{ cm}^{-1}$  peak, corresponding to DCPD, is shown in black. **d)** A line scan (blue line in **b)**) over the same area of the same sample after 24 h in the gelling solution.

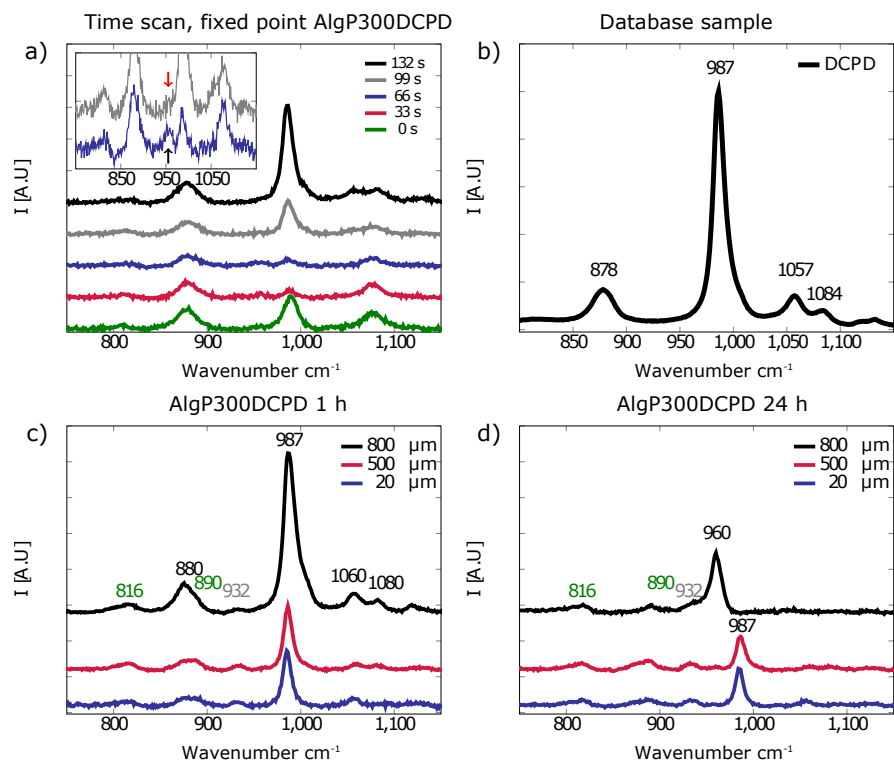


Figure 5: **a)** Raman spectra of an AlgP300DCPD sample from a single spot at 5 time points. The inset shows a close up of the 66 s and 99 s plots where a peak located at  $955\text{ cm}^{-1}$  is visible after 66 s (black arrow) and gone after 99 s (red arrow). **b)** Raman spectra of phase pure DCPD prepared in solution. **c)** and **d)** Raman spectra from a line scan of an AlgP300DCPD sample after 1 and 24 h respectively.

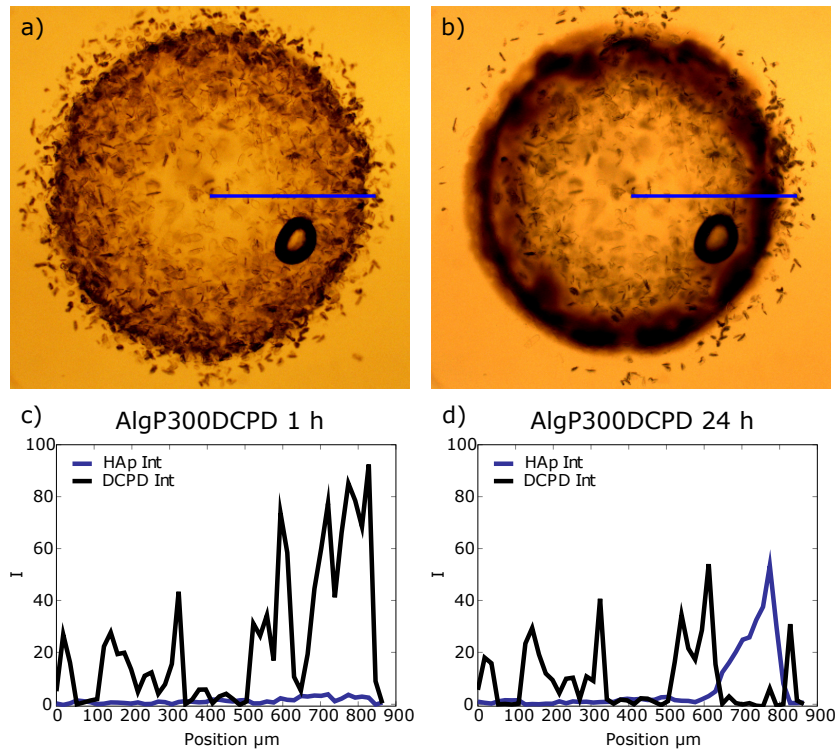


Figure 6: Optical images and Raman data for an AlgP300DCPD hydrogel disc ( $\varnothing \approx 1.6$  mm) gelled and mineralized in a 1 M calcium solution at pH 5. **a)** After 1 h in the gelling solution. **b)** After 24 h in the gelling solution. **c)** A line scan (shown by the blue line in **a)**) with the intensity of the  $960\text{ cm}^{-1}$  peak corresponding to HAp shown in blue and the intensity of the  $987\text{ cm}^{-1}$  peak, corresponding to DCPD, is shown in black. **d)** A line scan of the same sample after 24 h in the gelling solution.

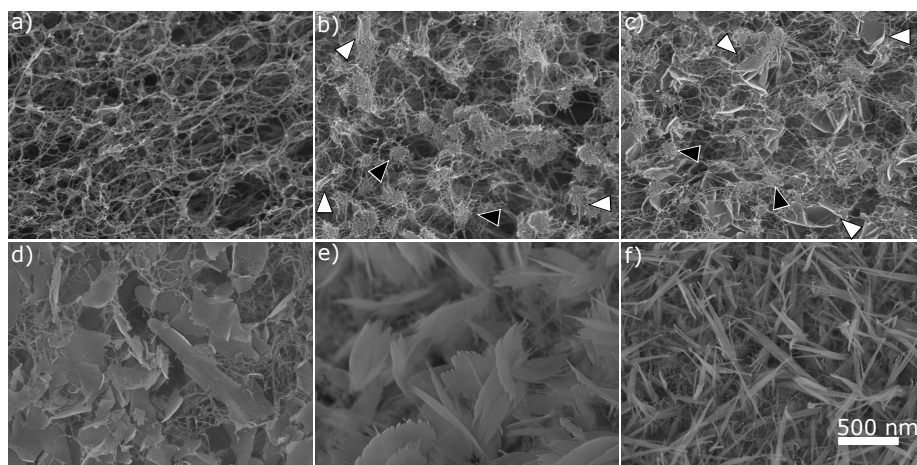


Figure 7: SEM-images of an AlgP300 sample gelled and mineralized in a 1 M  $\text{CaCl}_2$  solution at pH 5. **a)**, **b)** and **c)** are recorded from a sample incubated in the gelling solution for 1 h, while **d)**, **e)** and **f)** are recorded from a sample incubated in the gelling solution for 24 h. Black arrowheads indicate to selected alginate/mineral nodules. White arrowheads indicate selected flaky plate like crystals. The scale bar applies to all of the images in this figure.

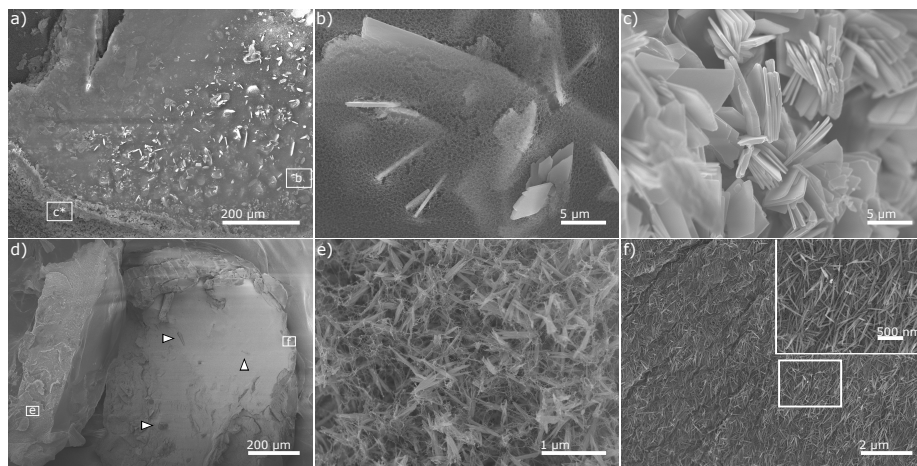


Figure 8: SEM-images of an AlgP300DCPD sample gelled and mineralized in a 1 M calcium solution at pH 5. The sample shown in **a**), **b**) and **c**) was incubated in the gelling solution for 1 h and shows large brushite crystals within the alginate network and a dense layer of crystals at the surface, seen in **c**). The sample shown in **d**) (this image is a collage of two separate images), **e**) and **f**) was incubated in the gelling solution for 24 h and shows a few remaining brushite crystals marked with white arrowheads and acicular HAp crystals within the alginate network. White boxes show the position of higher magnification images. The asterisk denotes the image was from a similar region in the sample geometry.

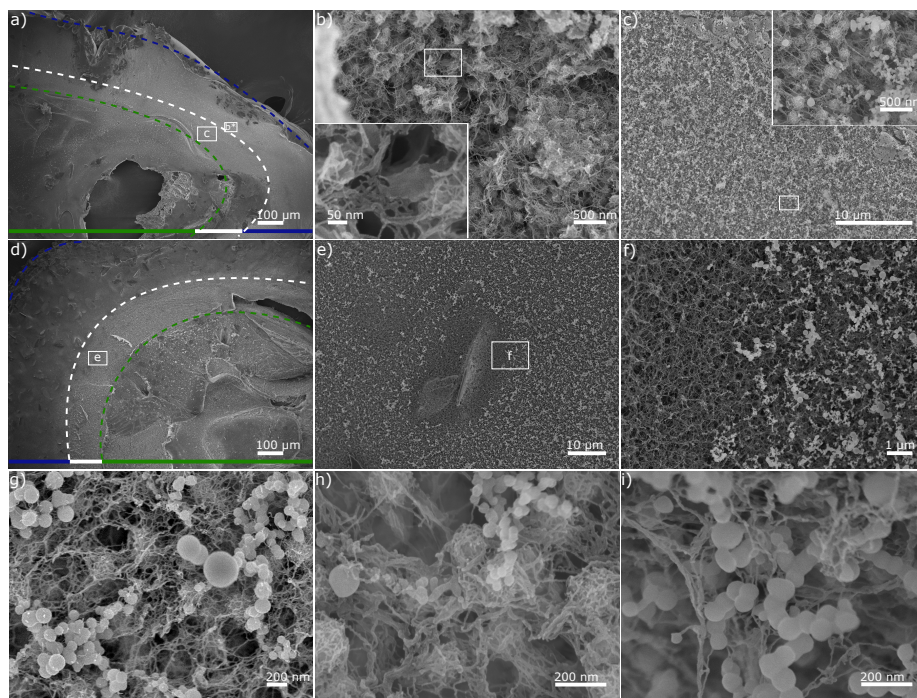


Figure 9: SEM images of an AlgP300 sample (**a**), **b**), **c**), **h**) and **i**)) and an AlgP300DCPD sample (**d**), **e**), **f**) and **g**)) gelled at pH 5 and arrested after 3 min reaction time. The image in **a**) shows a low magnification overview with the gelled, transient and ungelled regions marked with blue, white and green respectively. **b**) and **c**) are higher magnification images from the gelled and transient regions respectively. **d**) is a low magnification overview of a seeded sample with similar regions marked as in **a**). **e**) and **f**) are magnified images of an area surrounding a seed, showing how the metastable phase has been consumed by the crystal seed. Images **g**) (AlgP300DCPD made at pH 5), **h**) (AlgP300 made at pH5) and **i**) (AlgP300 made at pH7) show similar morphologies of particles found in the transient zone of samples made under different conditions. White boxes show the position of higher magnification images. The asterisk denotes the image was from a similar region in the sample geometry.

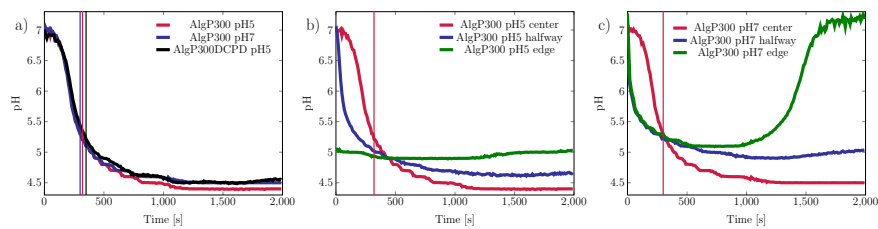


Figure 10: **a)** pH-data gathered from a  $121 \times 121 \mu\text{m}$  square in the center of discs produced under three different conditions (given in the legend). The vertical lines mark the time point at which the samples were gelled, as determined by optical microscopy. The graphs in **b)** and **c)** show AlgP300 samples subjected to gelling solution of pH 5 and pH7 respectively. The pH value was recorded (also  $121 \times 121 \mu\text{m}$  area averages) over time from 3 positions; at the edge close to the surrounding solution, at a point halfway into the disc and from the center. It can be seen in both conditions that the surrounding solution experiences a drop in pH followed by an increase back to the initial buffered pH. This phenomenon is more obvious in **c)**.

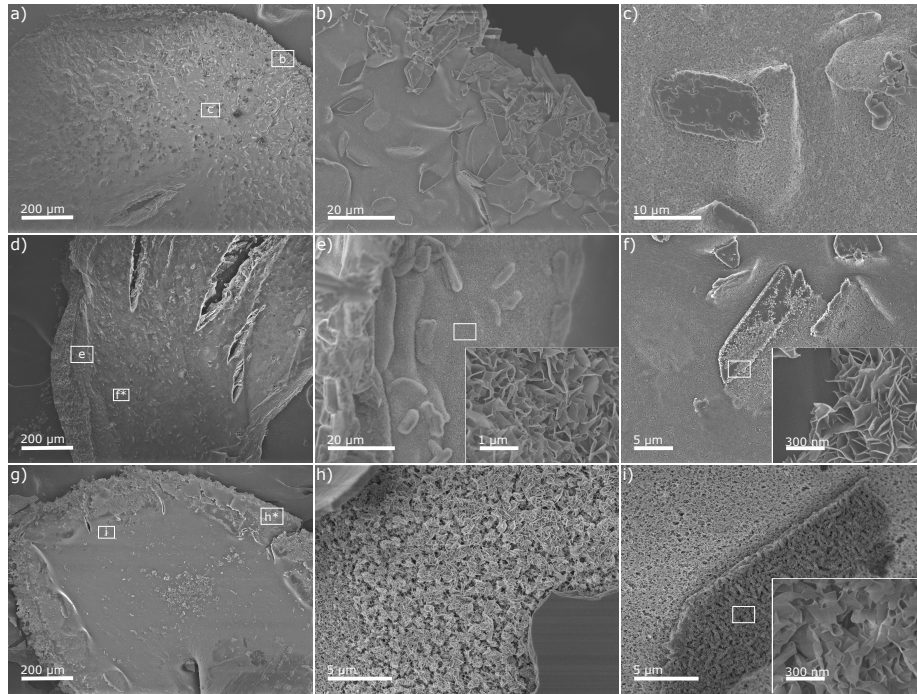


Figure 11: SEM images of an AlgP300DCPD sample after 0 h (**a-c**), 24 h (**d-f**) and 168 h (**g-i**) incubation in SBF. **a**), **d**) and **g**) show a low magnification overview images at the different time points. White boxes show the position of higher magnification images. The asterisk denotes the image was from a similar region in the sample geometry. **b**) shows the extensive growth of brushite crystals along the edge of a disc. **c**) shows a higher magnification image of brushite crystals present further into the disc. **e**) shows a region close to the edge of a disc where a uniform region of flaky HAp crystals (a high magnification image can be seen in the inset) is visible as well as areas where the morphology of previous brushite crystals has been converted into HAp. **f**) show the nucleation of HAp (seen as flaky crystals in the high magnification inset) close to and on the surface of a brushite crystal after 24 h incubation. **h**) shows a region close to edge after 168 h incubation where a uniform band of flaky HAp crystals could be seen. **i**) shows nanocrystals which have assumed the morphology of an initial brushite crystal.